Accepted Manuscript

Fibre failure assessment in carbon fibre reinforced polymers under fatigue loading by synchrotron X-ray computed tomography

S.C. Garcea, I. Sinclair, S.M. Spearing

PII: S0266-3538(16)30844-2

DOI: 10.1016/j.compscitech.2016.07.030

Reference: CSTE 6476

To appear in: *Composites Science and Technology*

Received Date: 4 March 2016

Revised Date: 22 June 2016

Accepted Date: 29 July 2016

Fibre failure assessment in carbon fibre reinforced polymers under fatigue loading by synchrotron X-ray computed tomography

S.C. Garcea[1]*, I. Sinclair[1], S.M. Spearing[1]

[1] Materials Research Group, Faculty of Engineering and the Environment, University of Southampton, Southampton, United Kingdom

* Corresponding author (scg1a09@soton.ac.uk)

Abstract

In situ fatigue experiments using synchrotron X-ray computed tomography ~~(SRCT)~~ are used to assess the underpinning micromechanisms of fibre failure in double edge notch carbon/epoxy coupons. Observations showed fibre breaks along the 0º ply splits, associated with the presence and failure of bridging fibres, as well as fibres failed in the bulk composite within the 0º plies. A tendency for cluster formation, with multiple adjacent breaks in the bulk composite was observed when higher peak loads were applied, exceeding 70% of the ultimate tensile stress. *Ex situ* fatigue tests were used to assess the accumulation and distribution of fibre breaks for different loading conditions, varying peak load and number of cycles. A direct comparison with the quasi-static case for an equivalent peak load, considering the same material system and geometry, has shown that fatigue produces a significantly higher number of fibre breaks. This supports the hypothesis that fibre breaks are indeed caused by the load cycling.

Keywords: A. Carbon fibre composite, B. Fatigue, C. Fibre failure, C. Damage mechanics, D. Synchrotron radiation computed tomography

1. Introduction

The issue of fibre failure under fatigue loading in carbon-fibre reinforced polymer composite materials has received relatively little attention. As composite materials are increasingly used in major structural applications such as civilian aircraft, wind turbines and pressure vessels in which durability is a key, it becomes important to understand the mechanisms which determine the economically useful life. It is generally understood that carbon fibres do not suffer degradation under cyclic loading [1,2], which may explain the lack of prior work. Although carbon fibre composites are relatively fatigue insensitive they generally do have downward sloping S-N curves and finite life under fatigue loading [3]. ~~However, f~~ Fibre failure is known to constitute the critical damage mechanism in tension, for which the axial strength of unidirectional composites is assumed to be controlled by the strength distribution of the fibres [4]. Several modelling approaches have been developed to predict fibre-dominated tensile strength, taking into account the fibre strength distribution [5], stress transfer around broken fibres [6-13], and the formation of clusters of fibre breaks [14,15]. None of these models have been extended to the case of fatigue loading. Both for the quasi-static case, and particularly for fatigue, there is a lack of direct observations of fibre failure which could be used to inform and validate predictive models. Green *et al.* [16] observed delamination-dominated failure (ply-level scaling) and fibre-dominated failure (sub-laminate level scaling) under quasi-static load depending on the quasi-isotropic configuration considered, albeit without direct observations of fibre failure. However, when the same material systems were considered under fatigue loading on a sub-laminate level, the observed failure modes were delamination-dominated, except for load levels higher than 90%, which showed fibre-dominated failure [17]. Wright *et al.* [18] observed fibre breaks in carbon/epoxy coupons subject to quasi-static loading by the use of high-resolution computed tomography, demonstrating that this technique can be used to visualise individual fibre failures, identify their location and the correlation with other damage modes. Scott *et al*. used the same technique to quantify fibre failure in coupons subjected to incremental quasi-static loading [19]. The results showed a progressively increasing rate of fibre fracture with load, which could be approximated by a power-law relationship, and an increasing tendency for fibre breaks to occur in clusters at high percentages of the failure load [19]. These observations were refined by Swolfs *et al.* [20], who noted that the tendency for cluster formation at high strains (>1.6%) accounted for 50% of the total breaks detected, and also that the majority of the clusters were co-planar (70%) rather than diffuse (30%). However, the model proposed overestimated the accumulation of fibre breaks, underestimated the cluster formation, and also predicted diffuse rather than co-planar clusters in contrast with the experimental observations [20]. The underestimation of cluster formation was also found to be a weakness of a different modelling strategy documented in work by Scott *et al.* [4]. The assessment of fibre breaks in composites under fatigue loading is not trivial due to the fact that *in situ* tests are highly desirable to monitor their accumulation. Previous work conducted by Spearing *et al.* [21] identified the presence of fibre breaks in centre-notched specimens subject to tension-tension fatigue by the use of scanning electron microscopy (SEM) on thermally-deplied specimens. Clusters of broken fibre were observed along the 0º ply split, with fibre breaks particularly concentrated at the intersection between 0º ply splits and transverse ply cracks [21]. However, the intrinsic limitation associated with the techniques available (radiography and SEM) did not allowed the assessment and mapping of fibre breaks within the ply thickness, and also does not provide assurance that some of the fibre breaks were not caused during the de-plying process.

The current work, to the best of the authors' knowledge, represents the first use of *in situ* fatigue experiments to assess the micromechanisms of fibre failure by the use of synchrotron X-ray computed tomography. The formation of fibre breaks along the 0º ply splits and within the bulk composite (in the 0º plies) has been quantified. A direct comparison with an equivalent quasi-static case has been provided, showing that the fibre breaks detected are associated with the cycling process.

2. Materials and methodology

A thermoplastic particle-toughened T700/M21 carbon/epoxy with 60% nominal volume fraction of fibre [19] and a $[90/0]_s$ layup was used. The material was laid up and autoclave cured using a standard aerospace cure cycle as specified by the supplier [22]. Double-edge notched specimens (Figure 1(a)), with a nominal central ligament between the notches of 1 mm, a width of 4 mm, lengths of 34 mm (*in situ* tests) and 66 mm (*ex situ* tests); were shaped by waterjet cutting. Further details on the geometry, coupon dimensions, and experimental setup are described in [23] for the *in situ* fatigue tests, and in [24] for the *ex situ* tests. The average ultimate tensile failure stress (UTS) was measured as 960 MPa across the notched cross-section [25] with a coefficient of variation of 0.03 [26]. *In situ* fatigue tests (R ratio = 0.1), performed at 0.05 Hz using a compact load frame, were used to assess the micromechanisms of fibre failure. A peak load of 50% UTS was used to cycle specimens, CT images were obtained at 700 and 800 cycles. The increment of 100 cycles allowed the damage to remain within the restricted field of view available (~1.5x1.5 mm) at the high imaging resolution. *Ex situ* fatigue tests were used to monitor the accumulation and the distribution of fibre breaks for a wider range of loading conditions, varying the peak load (30%-50%-70% UTS), and the number of cycles (10^3, 10^5, 10^6). *Ex situ* ~~E~~ experiments were performed using a standard servo-hydraulic load frame, with a load ratio of R=0.1 and a frequency of 10 Hz. *In situ* and *ex situ*-loaded coupons were scanned at the Swiss Light Source (on the TOMCAT-X02DA Beamline, Paul Scherrer Institut, Switzerland). The beam energy was 19 keV and the distance between the specimen and detector was 30 mm; providing a degree of phase contrast. Specimens were placed in the load frame and scanned under load, applying 90% of the peak load used during the fatigue tests. The voxel resolution was chosen accordingly with the objective of the study: 0.69 μm was used for the *in situ* tests to facilitate the identification of the micromechanisms of fibre failure, while 1.6 μm was used for the *ex situ* experiments, allowing a larger field of view, but still reasonable resolution for fibre break detection [19]. Three-dimensional reconstruction was obtained from radiographs using an in-house code based on the GRIDREC/FFT approach [27]. The scanned volume of the *in situ* coupons located at the middle of the notch-center and up to 1.5 mm on one side of the notch (as shown in Figure 1~~(a)~~ (b)), was maintained the same between the two cycling conditions (700 and 800 cycles) to facilitate registration. The reference volume used for the *ex situ* tests was larger, corresponding to the lower voxel resolution, starting from the middle of the notch and extending for a length of 3 mm, Figure 1(c) ~~(b)~~. The reason for assessing fibre breaks over a wider region than the 'geometrical notch region' was dictated by the fact that matrix-dominated damage and fibre fracture is not limited to the notch region, but occurs over a larger volume [28]. Therefore, in this study the term '*notch region*', does not strictly correspond to the geometrical notch, but to an extended region (~3 mm in length) as shown in Figure 1(c) ~~(b)~~. The distribution of fibre breaks along the 0º ply split path has been evaluated, taking into account the total length of the split associated with the different loading conditions (variation of load and/or cycles) to enable the measurement of the fibre break density in the wake of the crack tip. In these cases multiple scans were concatenated to include all the damage, up to a length of 12 mm, as shown in Figure 1(d) ~~(c)~~, which corresponds with 6 scan volumes joined together. Volume concatenation was performed using the open source software ImageJ, while fibre breaks were detected and analysed by the use of the commercial software VGStudio Max v2.1. Fibre breaks were visually inspected using all three orthogonal planes to avoid ambiguity with local matrix microcracks and to ensure accuracy of the measurements the values provided are based on three separated counts made on different occasions. The distribution of the fibre breaks along the 0º ply splits ~~(Figure 4 and 5)~~, defined as fibre break density, was assessed along 0.5 mm sections of crack by counting the number of fibres failed (*i.e.* number of breaks/0.5 mm of crack length).

3. Results and discussion

3.1 Observations of fibre failure

Table 1 summarises the fibre breaks detected for the different loading conditions investigated. As noted previously, the notch region is represented by a length of 3 mm from the middle of the notch towards one of the specimen ends, while the '*split volume'* refers to the volume defined by the whole length of the 0º ply splits. Therefore, care needs to be taken in comparing these values within the 'notch region', which ensures that the same volume for all the cases is considered. However, the number of fibre breaks within the split volume provides the overall number of fibre failed detected for each single loading condition.

3.2 Micromechanisms of fibre failure

A previous study conducted under fatigue loading using the same material system has shown that 0º ply split propagation in fibre-packed regions occurs principally at the fibre matrix interface [24]. The current work investigates the micromechanisms of fibre fracture observed along the 0º ply split paths using *in situ* fatigue tests. The comparison of the two cyclic conditions (700 and 800 cycles at 50% UTS) has shown twelve additional fibres breaks in this small region (~1x1.5x1 mm) occurring during the increment of 100 cycles, in addition to the 74 fibres that had already failed at 700 cycles. The fragmented fibres observed are all located along the planes of the 0º ply splits, and most of the additional breaks appear as single breaks (10), with one doublet (two adjacent fibre breaks). Depending on the direction of the fibre bridging (with respect to the damage propagation), and on the direction of the shear, two fibre failure modes have been identified, shown in Figure 2. In these two cases crack cross-sections parallel to the loading direction have been considered, and the image at 800 cycles is registered to the same position in the coupon as at 700 cycles. The 0º ply split propagates at the fibre/matrix interface at 700 cycles (Figure 2(a) and 2(c)) creating a partial debonding of the fibre, which is connected to the adjacent matrix in an asymmetric way with respect to the split propagation. The traction associated with the crack opening (perpendicular to the load direction) acts on the fibre causing local bending, visible in Figure 2(c). The next cyclic increment (800) shows the failure of the fibre in Figure 2(b) and 2(d). The fibre does not fail when it interacts with the damage propagation in the first instance, but as consequence of the increasing shear and bending, acting on the debonding fibre. This mechanism represents a wake process rather than a near-tip process. The direction of the shear, Figure 2(a), indicates that the failure of the fibre is due to tensile stress in this particular case. However, in the same coupon fibre failure due to local compression resulting in a highly localised buckling process has also been detected (Figure 2(d), consistent with the opposite shear direction shown in Figure 2(c). Again, in these two images, the same position in the specimen is viewed for 700 and 800 cycles. The comparison between Figure 2(b) and Figure 2(d) clearly displays fracture planes perpendicular to the load for the tensile failure (Figure 2(b)), whereas the fibre break due to local buckling is orientated at 45º with respect to the loading direction (Figure 2(d)). In addition, differences in terms of the opening between the fracture surfaces of the fibre have been observed for the two cases: the buckling failure shows fracture surfaces close to each other, Figure 2(d); while those associated with the tensile failure are separated by a greater distance, Figure 2(b). Considering that 0º ply split propagation is mode II dominated, this difference is consistent with the stress acting on the fibre, which is in compression in the buckling failure and in tension in the tensile failure. The analysis conducted has shown that the additional fibre breaks detected at 800 cycles along the 0º ply split do not occur adjacent to pre-existing fibre breaks, but in new locations. The number of fibres failed in buckling and in tension detected along the 0º ply splits is the same (exactly 37 of each) at 700 cycles, while the additional fibre breaks observed at 800 cycles are predominantly due to buckling (11) rather than tension (1). Given the small numbers of broken fibres involved, further work would be needed to assess the significance of this observation. However, the balance between the number of fibre breaks due to buckling and tension is of interest, and provides insight regarding the micro-mechanisms of failure and has the potential to inform the development of models for failure.

Observations conducted on the *ex situ* fatigue tests for different loading conditions have confirmed the micromechanisms detected for the *in situ* experiments. Figure 3 shows an example from an *ex situ* test of fibre buckling that involves two adjacent fibres and a single fibre located a few fibre diameters apart along the split path, which resulted in local fibre kinks. Two co-planar fibre break doublets, located within the composite, close to the 0º ply split path have also been detected, and may be a result of stress transfer from the compressive failures.

3.3 *Ex situ* results for fibre failure along the 0º ply splits

The *in situ* fatigue experiments documented in the previous section have identified the failure of oblique bridging fibres as the main mechanism of fibre failure along the 0º ply splits. However, performing *in situ* fatigue tests limits the number of cycles that can be applied given the modest loading frequency available. As such, the imaging of *ex situ* fatigue-loaded coupons provides the opportunity to investigate a wider range of loading conditions (load levels and numbers of cycles) in order to augment the observations made via the *in situ* tests. This technique is better able to measure fibre break density and the distribution of failed fibres along the 0º ply splits as a function of the number of cycles, peak loads and crack length, including the whole splitting region. Figure 4 shows ~~results~~ the fibre break distribution along the 0º ply split obtained for a high number of cycles (10^6) with a low peak load (30% UTS), and for an intermediate load (50% UTS) and a low number of cycles (10^3). The distance along the split is measured from the root of the crack, located at the notch, while the crack tip for the two cases is highlighted on the graph by a dashed line. The crack length detected for these two loading conditions is similar (~3 mm). The total number of fibre breaks observed ~~along the 0º ply split~~ for the case of 50% UTS is considerably higher than the 30% UTS case, notwithstanding the high number of cycles applied for the latter. Similarities can be observed from a direct comparison between these two loading conditions, as shown in Figure 4:

- The fibre break density increases with the distance away from the crack tip. As such, the root of the cracks exhibit the highest number of fibre breaks, consistent with fibre failure being primarily linked to fibre bridging in the wake.
- No fibre breaks were observed within 0.5 mm of the crack tip, again indicative of fibre fracture being a wake phenomenon, and not being driven by local crack tip stresses.
- No fibre breaks have been detected ahead of the crack tip.

Figure 4 shows that for a given total crack length the fibre failure density distribution along the split path is strongly influenced by the peak load, resulting in higher values of fibre break density at equivalent locations relative to the crack tip for the higher load case. Further increases in the peak load and/or the number of cycles (for loads equal or higher than 50% UTS) result in an increase of fibre breaks along the 0º ply split. Figure 5 shows the results obtained for an intermediate peak load (50% UTS) at 10^5 cycles compared with a higher peak load (70% UTS) at a lower number of cycles (10^3). The two data sets show similar overall trends from the crack tip back to the root of the crack. For both load cases, the fibre break densities along a given crack wake appears to 'saturate' with increasing distance from the crack tip (at a value of ~25 breaks/0.5mm), particularly in the 50% UTS case. In the 70% case this also occurs but is complicated by a number of local peaks in break density (>30 breaks/0.5mm). These peaks were found to be associated with clusters of fibre breaks in the 70% UTS case, which is discussed in the following section. In the first instance, this suggests that the maximum number of fibres available for fracture across the crack width is limited, presumably linked to the microstructural arrangement of the fibres (*e.g.* the presence of occasional mis-oriented fibre which are available to cause bridging of a bulk fibre-interface driven intralaminar crack). The saturation value of ~25 breaks/0.5mm is similar to the value observed near the crack root for the intermediate load (50% UTS) and low number of cycles (10^3) shown in Figure 4. Therefore, the increase in the number of cycles (from 10^3 to 10^5) for a fixed peak load (50% UTS) does not appear to contribute to the development of more fibre fractures at the root of the 0º ply split, but it does cause an increase in fibre break density along the entire crack length (see Figure 4 and Figure 5 for comparison). Both the increase in the number of cycles for the intermediate load (50% UTS) and the application of a higher peak load (70% UTS), even for a low number of cycles, are responsible for cluster formation along the 0º ply split. The largest cluster consisted of twenty adjacent fibre fractures, observed along one of the 0º ply splits in the specimen cycled at 50% UTS and 10^5 cycles. Figure 6 shows a cross-section parallel (Figure 6(a)) and perpendicular (Figure 6(b)) to the loading direction for this cluster. Two branches of the crack propagate parallel to the loading direction for a ply thickness of ~50 µm, and they interact with the delamination. The use of an *ex situ* experiment, as in this case, does not allow clarification as to whether the cluster of twenty fibre breaks, which is located between the two branches of the split and delamination is associated with the coalescence of damage or due to a similar crack wake process, albeit involving more fibres, as observed in Figure 2. However, analysis is limited here to the presence of a single dominant 0˚ ply split, which was observed in the great majority of cases, as opposed to occasional bifurcation of a given ply crack.

3.4 Fibre failure in the bulk composite

The application of an intermediate load, (e.g. 50% UTS) coupled with more than 10^3 cycles equal or higher peak loads (e.g. 70% UTS), resulted in fibre failure in the bulk composite, away from splits and delamination, see Table 1. The comparison of the number of fibre breaks detected within the 0º plies is referred to here as the 'notch region', which is defined by a nominal gauge length of 3 mm, measured from the middle cross-section of the notch, see Figure 1(b). The case of 50% UTS and 10^3 cycles exhibits a low number of fibre breaks in the bulk: seven were identified, where three appear as singlets (single fibre breaks), and two as doublets. The doublets consisted of co-planar fibre breaks, as shown in Figure 3. The increase in the number of cycles (10^5) for the same peak load (50% UTS) corresponds to a slight increase in the total number of fibre breaks in the bulk (18), the majority occurring as singlets (14), and a few co-planar doublets (2). The distribution of fibre breaks in the bulk with respect to the position of the 0º ply splits for this latter loading case is shown in Figure 7(a), where the volume defined by the 0º ply split lengths has been considered, concatenating three scans. Fibres failed in the bulk are located within the region bounded by the 0º ply splits and the delamination, where the local stress is expected to be raised due to the load-bearing cross section being reduced by the presence of splits and delamination. While split growth reduces the load bearing cross-section along the 0º ply width, the delamination separates the 0º from the 90º plies, as shown in a typical cross-section perpendicular to the loading direction in Figure 8. This is consistent with the observation that no fibre breaks have been detected ahead of the crack tips (Figure 7(a)) and outside of the region of interest delimited by the 0º ply splits and by the delamination (Figure 8). The majority of fibres failed as singlets (in blue), consistent with the results found for the same peak load and lower number of cycles (10^3). Therefore, for the intermediate peak load, the increase in cycles does not contribute to the preferential formation of clusters. It is interesting to note that the fibre breaks are distributed throughout the volume delimited by the 0º ply splits, not exclusively within the notch region. The presence of transverse ply cracks, two of which are located in a symmetric position in the notch region, indicated by a dark grey line perpendicular to the loading direction in Figure 7(a), apparently do not have a major effect on the location of fibre breaks, contrary to previous studies in which breaks were found to correlate with transverse ply cracks [18,21]. The application of a higher peak load, 70% UTS, results in a significant number of fibre breaks in the bulk (70) within the notch region, even for a low number of cycles (10^3), see Table 1. Figure 7(b) shows the three-dimensional map of fibre failure locations for this loading condition, where the notch region (dark grey volume) has been concatenated with an additional volume (light grey). The remaining volume corresponding to the 0º ply split continuation, located at 6 mm from the middle of the notch and extended for further 3 mm, has not been included in the rendering for easier visualisation. However, the analysis conducted has shown only two fibre breaks in the bulk located out of the field of view shown, both in the region of interest already identified (between the 0º ply splits and the delamination), with the majority of the breaks lying in the volume shown in Figure 7(b). It is clear that the application of high peak loads increases the tendency for cluster formation. Clusters consisting of up to five co-planar broken fibres were detected (Figure 7(b)), while the intermediate load shows exclusively singlets and doublets, Figure 7(a). The fibre break distribution for loading at 70% UTS shows apparently the accumulation in two main regions: the notch region located in the first millimetre from the middle of the notch, and an intermediate region between 2 and 4 mm from the middle of the notch. However, further analyses to investigate these two locations characterised by higher fibre breaks density in the bulk do not show any differences and/or connections with other damage modes or with the local microstructure.

4. Comparison with the quasi-static case

In order to provide a comparison, fibre breaks for an equivalent quasi-static load of 80% UTS have been counted. The same measurement volume was used as in the fatigue cases, in terms of dimensions and location. In this measurement a total of 124 fibres were observed to have failed, with 14 breaks in the bulk composite, see Table 1. The fibre break density along the 0º ply split was calculated following the same procedure used for the fatigue cases, and the results are shown in Figure 9. Fibre break density increases from the tip towards the root of the split, showing a higher value at the root for the longer split. In addition, this latter case does not exhibit any fibre breaks over the 1.5 mm nearest the crack tip, which represents half of the crack length. The comparison between the quasi-static case (Figure 9) and the fatigue case at an intermediate peak load with low number of cycles (Figure 4) shows a similar trend. However, when higher peak loads and/or number of cycles were considered the fatigue cases exhibit a different trend, with a saturation of fibre breaks along the split (Figure 5). Both loading conditions (quasi-static and fatigue) do not result in fibre breaks in the immediate region behind the crack tip, suggesting that fibre failure along the 0º ply split is a wake-process for both cases. The level of fibre breaks in the wake (~20-25 breaks/0.5mm) is of the same order for both the quasi-static (Figure 9) and fatigue cases (Figure 4-5), consistent with the limiting number of fibre bridges formed being a function of the fibre distribution. Even though the maximum quasi-static peak load (80% UTS) was higher than the corresponding fatigue case (70% UTS), the number of fibre breaks is lower along the static 0º ply split and in the bulk, see Table 1. This is consistent with the observation that most fibre breaks occurring in the fatigue cases are associated with the cycling process and not with the initial quasi-static load. The clustering of fibre breaks in quasi-static loading are restricted to singlets (4) and doublets (5), in approximately equal proportion; and they are all located close to the 0º ply splits or to the ply interface. No delamination was detected for the quasi-static loading case.

5. Conclusions

The use of ~~SRCT~~ synchrotron radiation computed tomography has provided novel insights regarding fibre fracture in a polymer matrix composite under fatigue loading that had been hitherto impossible to achieve by other means. *In situ* and *ex situ* fatigue tests were used to investigate micromechanisms of fibre failure and to quantify the fibre break distributions. The loading conditions considered have shown fibre breaks along the 0º ply splits, mainly associated with the failure of bridging fibres. Their distribution along the 0º ply splits showed a different trend from the crack tip towards the root depending on the peak load and number of cycles applied. However, no fibre breaks have been detected in the region immediately behind and ahead the crack tip, consistent with this class of fibre fracture being associated with a wake-process failure. Fibres also failed in the bulk composite within the 0º plies at peak loads higher than 50% UTS. A greater tendency for cluster formation at peak load of 70% UTS has been observed. As yet the mechanism for fatigue fibre failure in the bulk composite, and its effect on residual strength is not understood. The results presented in this work provide novel insights regarding the role of fatigue on fibre fracture in carbon fibre polymer matrix composites. As composite structures are required to stay in service for increasing lifetimes, the issue of assessing residual strength and remaining life will only grow in importance. This work has the potential to provide a foundation for a new approach to addressing these issues.

Acknowledgements

The authors would like to acknowledge funding from AFOSR-EOARD, grant 113040, Programme Monitor: Lt. Col. Randall Pollak, also funding from EPSRC, grant EP/H1506X/1. The authors are grateful to the Swiss Light Synchrotron Radiation for access to the TOMCAT-X02DA beamline, and for the assistance of Dr. Sarah Irvine. Thanks are due to µ-VIS at the University of Southampton for the computer analysis facilities. Materials were supplied via Airbus SAS.

References

[1] Bunsell AR, Somer A. The tensile and fatigue behaviour of carbon-fibres. Plast Rub Compos Pro 1992; 18: 263-267.

[2] Kerr M, Chawla N, Chawla KK. The cyclic fatigue of high-performance fibers. Journal of The Minerals, Metals and Materials Society 2005; 57: 67-71.

[3] Harris B. Fatigue in Composites: Science and Technology of the Fatigue Response of Fibre-Reinforced Plastics. Woodhead Publishing, 2003.

[4] Scott AE, Sinclair I, Spearing SM, Thionnet A, Bunsell AR. Damage accumulation in a carbon/epoxy composite: comparison between a multiscale model and computed tomography experimental results. Compos Part A-Appl S 2012; 43: 1514-1522.

[5] Rosen B. Tensile failure of fibrous composites. AIAA J 1964; 2: 1985-1991.

[6] Zweben C. Tensile failure of fibers composites. AIAA J 1968; 6: 2325-31.

[7] Zweben C, Rosen BW. A statistical theory of material strength with application to composite materials. J Mech Phys Solids 1970; 18: 89-206.

[8] Hedgepeth JM. Stress concentrations in filamentary structures. NASA TND882 1961; Langley Research Center.

[9] Hedgepeth JM, Van Dyke P. Local stress concentrations in imperfect filamentary composite materials. J Compos Mater 1967; 1: 294-309.

[10] Harlow DG, Phoenix SL. The chain-of-bundle probability model for the strength of fibrous materials I: analysis and conjectures. J Compos Mater 1978; 12: 195-213.

[11] Harlow DG, Phoenix SL. Probability distributions for the strength of composite materials I: two-level bounds, Int J Fract 1981, 17: 347-372.

[12] Goree JG, Gross R. Stress in a three-dimensional unidirectional composite containing broken fibers. Eng Fract Mech 1980; 13: 395-405.

[13] Ochiai S, Schulte K, Peters PWM. Strain concentration for fibers and matrix in unidirectional composite. Compos Sci Technol 1991; 41: 237-256.

[14] Batford SB. Tensile strength of unidirectionally reinforced composites. I J Reinf Plast Compos 1982, 1:153-163.

[15] Smith RL, Phoenix SL, Greenfield MR, Henstenburg RB, Pitt RE. Lower-Tail approximations for the probability of failure of three-dimensional fibrous composites with hexagonal geometry. P Roy Soc Lond A Mat 1983; 388: 353-391.
[16] Green BG, Wisnom MR, Hallett SR. An experimental investigation into the tensile strength scaling of notched composites. Compos Part A–Appl S 2007; 38: 867-78.
[17] Nixon-Pearson OJ, Hallett SR. An investigation into the damage development and residual strengths of open-hole specimens in fatigue. Compos Part A–Appl S 2015; 69: 266-278.
[18] Wright P, Fu X, Sinclair I, Spearing SM. Ultra high resolution computed tomography of damage in notched carbon fiber-epoxy composites. J Compos Mater 2008; 42: 1993-2002.
[19] Scott AE, Mavrogordato M, Wright P, Sinclair I, Spearing SM. In situ fibre fracture measurement in carbon-epoxy laminates using high resolution tomography. Compos Sci Technol 2011; 71: 1471-1477.
[20] Swolfs Y, Morton H, Scott AE, Gorbatikh L, Reed PAS, Sinclair I, Spearing SM, Verpoest I. Synchrotron radiation computed tomography for experimental validation of a tensile strength model for unidirectional fibre-reinforced composites. Compos Part A-Appl S 2015; 77: 106-113.
[21] Spearing SM, Beaumont PWR. Fatigue damage mechanics of composite materials. I: Experimental measurement of damage and post-fatigue properties. Compos Sci Technol 1992; 44: 159-168.
[22] Hexcel HexPly M21. http://www.hexcel.com/Resources/DataSheets/Prepreg-Data-Sheets/M21_global.pdf
[23] Garcea SC, Sinclair I, Spearing SM. In situ synchrotron tomographic evaluation of the effect of toughening strategies on fatigue micromechanisms in carbon fibre reinforced polymers. Compos Sci Technol 2015; 109: 32-39.
[24] Garcea SC, Mavrogordato MN, Scott AE, Sinclair I, Spearing SM. Fatigue micromechanism characterisation in carbon fibre reinforced polymers using synchrotron radiation computed tomography. Compos Sci Technol 2014; 99: 23-30.
[25] Wright P, Moffat A, Sinclair I, Spearing SM. High resolution tomographic imaging and modelling of notch tip damage in a laminated composite. Compos Sci Technol 2010; 70: 1444-1452.
[26] Wright PM. Investigation of damage in laminated carbon fibre composites using high resolution computed tomography. PhD Thesis, University of Southampton; 2011.
[27] Dowd BA, Campbell GH, Marr RB, Nagarkar V, Tipnis S, Axe L, Siddons DP. Developments in synchrotron x-ray computed tomography at the National Synchrotron Light Source. Proc. SPIE 3372 1999; 224-236.
[28] Spearing SM, Beaumont PWR. Fatigue damage mechanics of composite materials Part III: Prediction of post-fatigue strength. Compos Sci Technol 1992; 44: 299-307.

Table Caption

Table 1 Summary of the fibre breaks detected for the fatigue and quasi-static cases investigated. The notch region is referred to a 3 mm length from the middle of the notch, while the split volume includes all the volumes defined by the 0º ply split length.

Figure Captions

Fig. 1 Coupon geometry (a) and schematic of the reference volume used for: (b) *in situ* tests; (c) notch region considered in the *ex situ* experiments; (d) example of the extended volume (multiple concatenation) to include the full 0º ply split length.

Fig. 2 0º ply split propagation along the fibre interfaces at 50% UTS and 700 cycles (a, c), and fibre failure at 800 cycles (b, d).

Fig. 3 Fibre breaks along the 0º ply split and as co-planar breaks in the bulk composite for a peak load of 50% UTS and 10^3 cycles.

Fig. 4 Fibre break density along the 0º ply split for the cases of: 30% UTS and 10^6 cycles, and 50% UTS with 10^3 cycles, both specimens have splits of similar length.

Fig. 5 Fibre break density along the 0º ply split for 50% UTS and 10^3 cycles, and 50% UTS with 10^5 cycles.

Fig. 6 Cluster of 20 fibre breaks near the 0º ply split detected at 50% UTS and 10^5 cycles: cross-section parallel (a) and perpendicular (b) to the loading direction.

Fig. 7 3D Distribution of fibre breaks in the bulk composite for: (a) peak load of 50% UTS and 10^5 cycles, (b) peak load of 70% UTS and 10^3 cycles.

Fig. 8 Cross-section of the coupon loaded at 50% UTS 10^5 cycles in the direction perpendicular to the load.

Fig. 9 Fibre breaks density along the 0º ply split for a quasi-static load of 80% UTS.

		Breaks along 0° ply split		Breaks in the bulk composite	
%UTS	**N (Cycles)**	Notch region	Split volume	Notch region	Split volume
30	**10^6**	57	57	-	-
50	**10^3**	148	148	7	7
50	**10^5**	325	542	18	33
70	**10^3**	363	700	70	107
80	**1 (Q-static)**	110	110	14	14

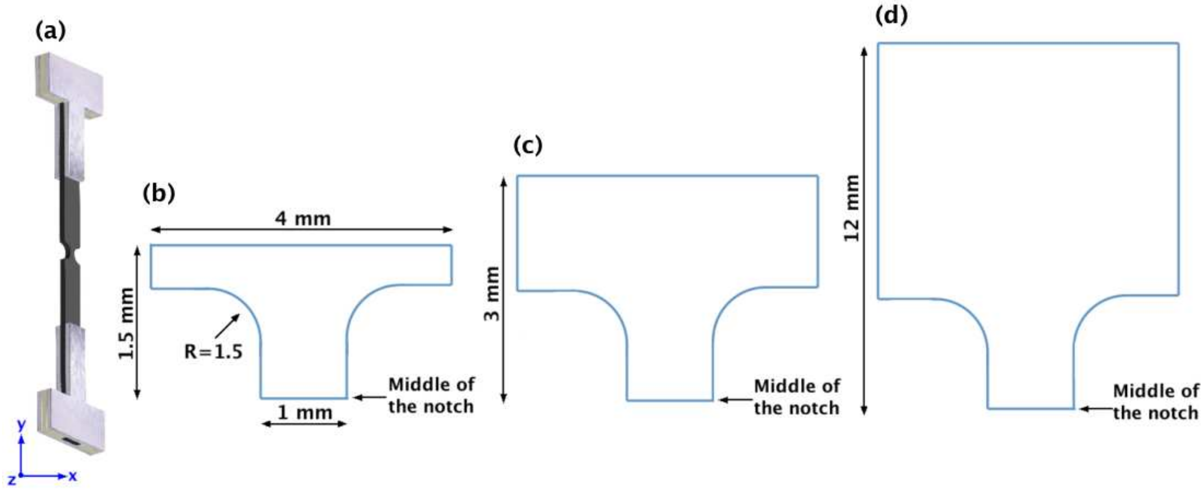
(a)
y
z
x
(b)
4 mm
1.5 mm
R=1.5
1 mm
Middle of
the notch
(c)
3 mm
Middle of
the notch
(d)
12 mm
Middle of
the notch

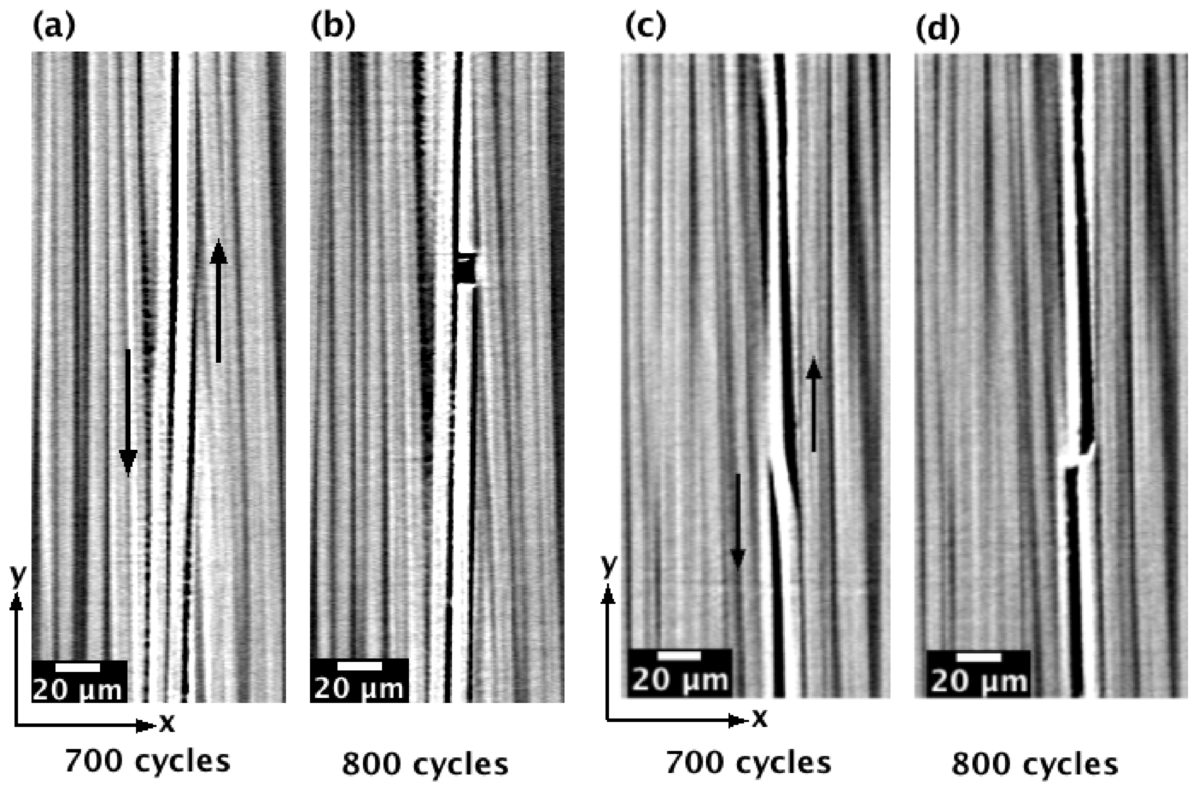
(a)
(b)
(c)
(d)
20 µm
20 µm
20 µm
20 µm
y
x
y
x
700 cycles
800 cycles
700 cycles
800 cycles

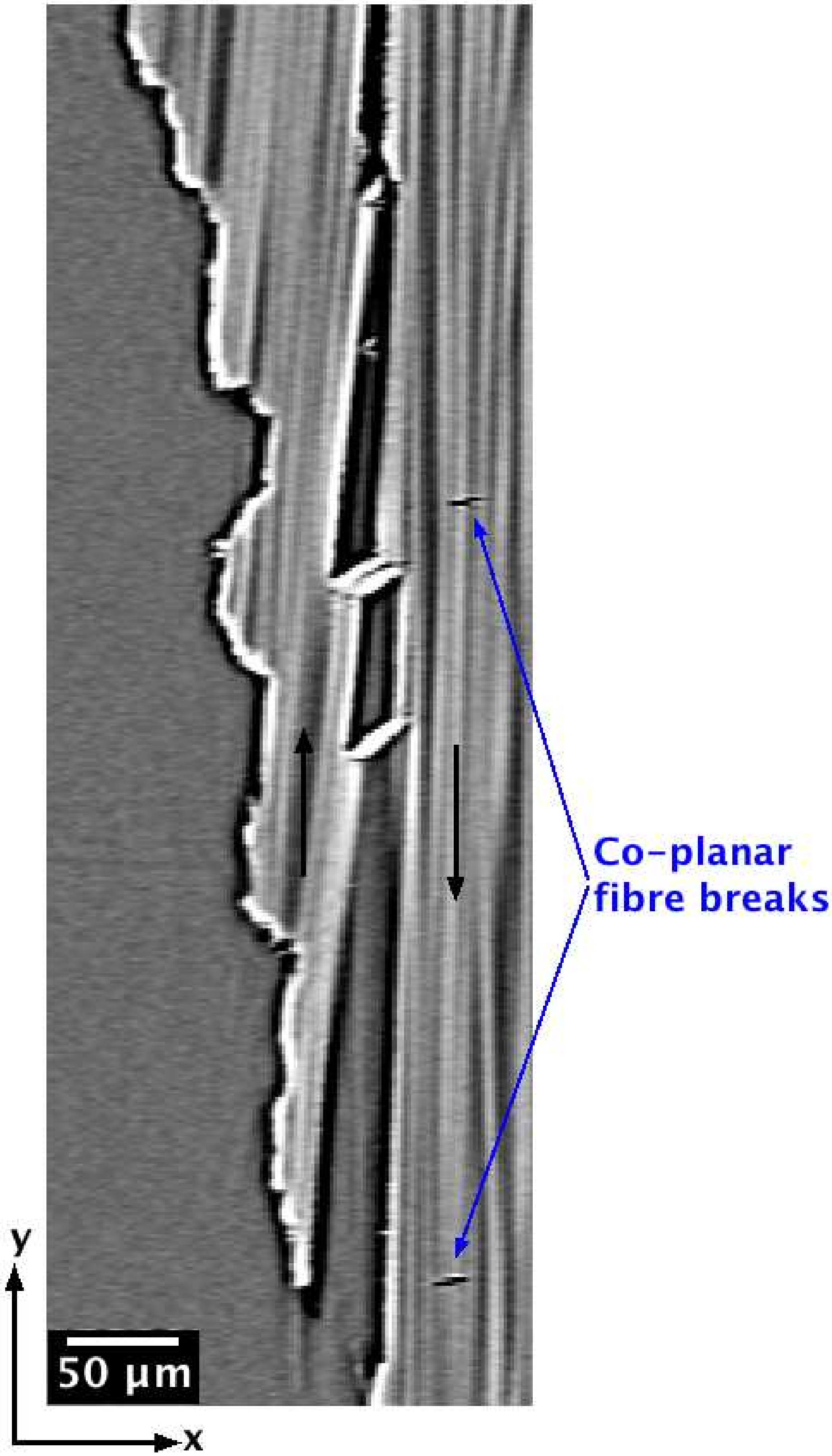
Co-planar
fibre breaks
50 µm
y
x

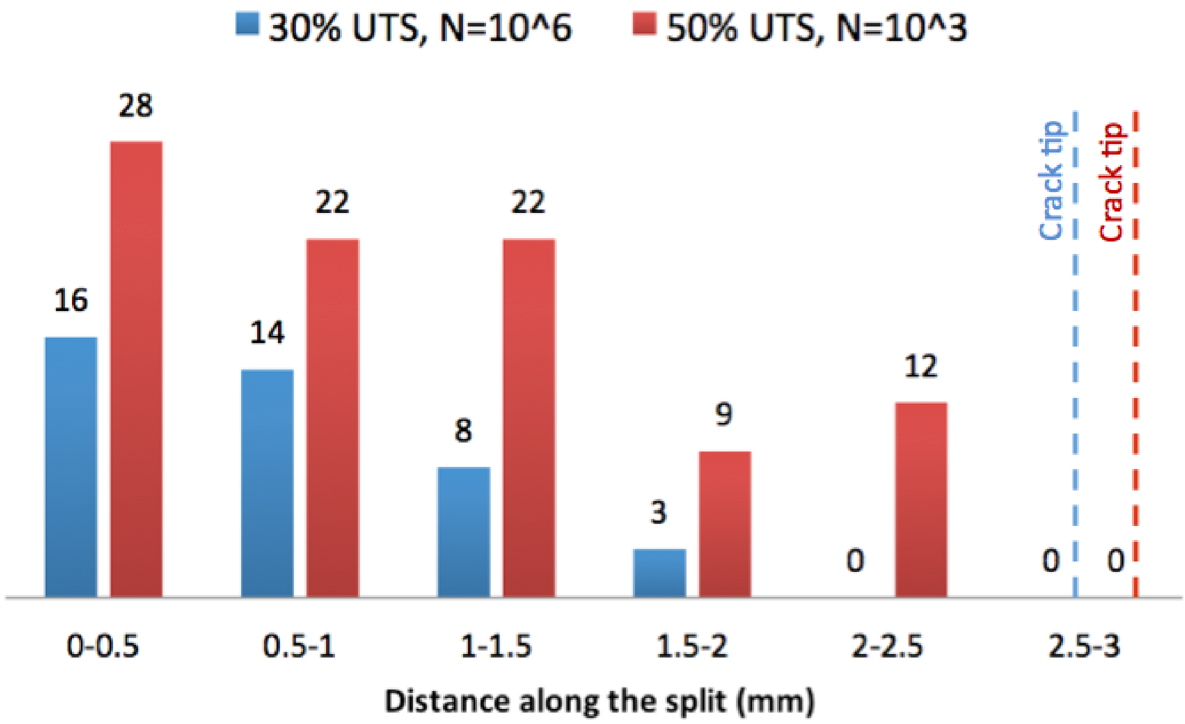
30% UTS, N=10^6
50% UTS, N=10^3
28
16
22
14
22
8
9
3
12
0
0
0
Crack tip
Crack tip
0-0.5
0.5-1
1-1.5
1.5-2
2-2.5
2.5-3
Distance along the split (mm)

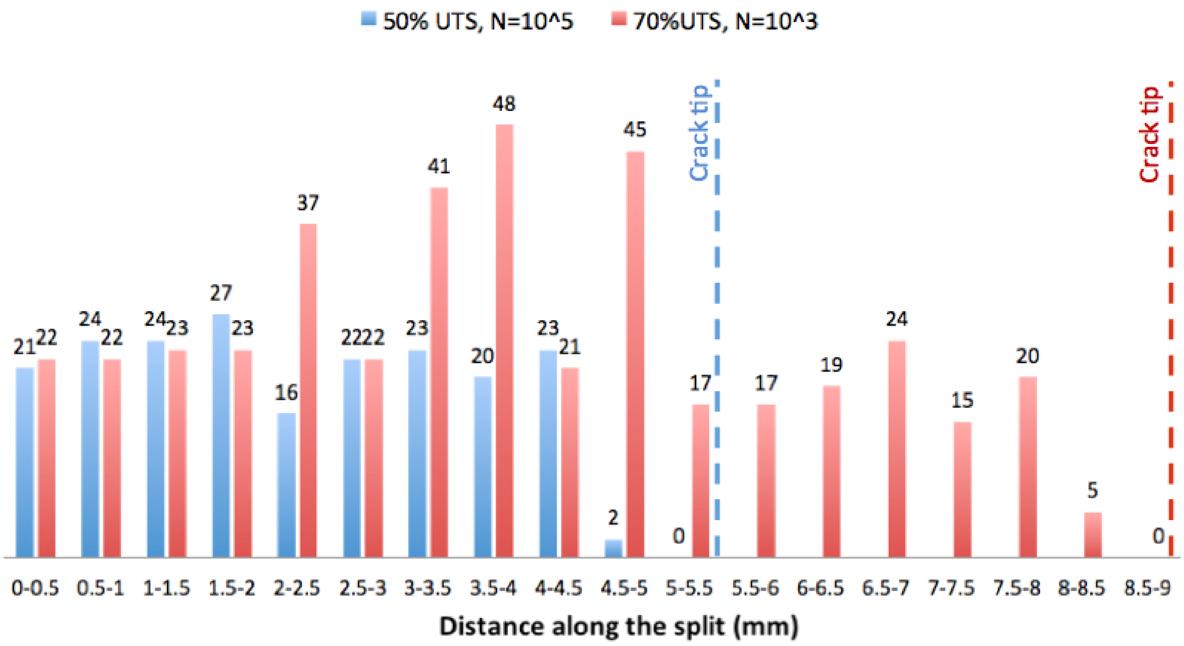
50% UTS, N=10^5
70%UTS, N=10^3
Crack tip
Crack tip
21 22
24 22
24 23
27 23
16 37
22 22
23 41
20 48
23 21
2 45
0 17
17
19
24
15
20
5
0
0-0.5
0.5-1
1-1.5
1.5-2
2-2.5
2.5-3
3-3.5
3.5-4
4-4.5
4.5-5
5-5.5
5.5-6
6-6.5
6.5-7
7-7.5
7.5-8
8-8.5
8.5-9
Distance along the split (mm)

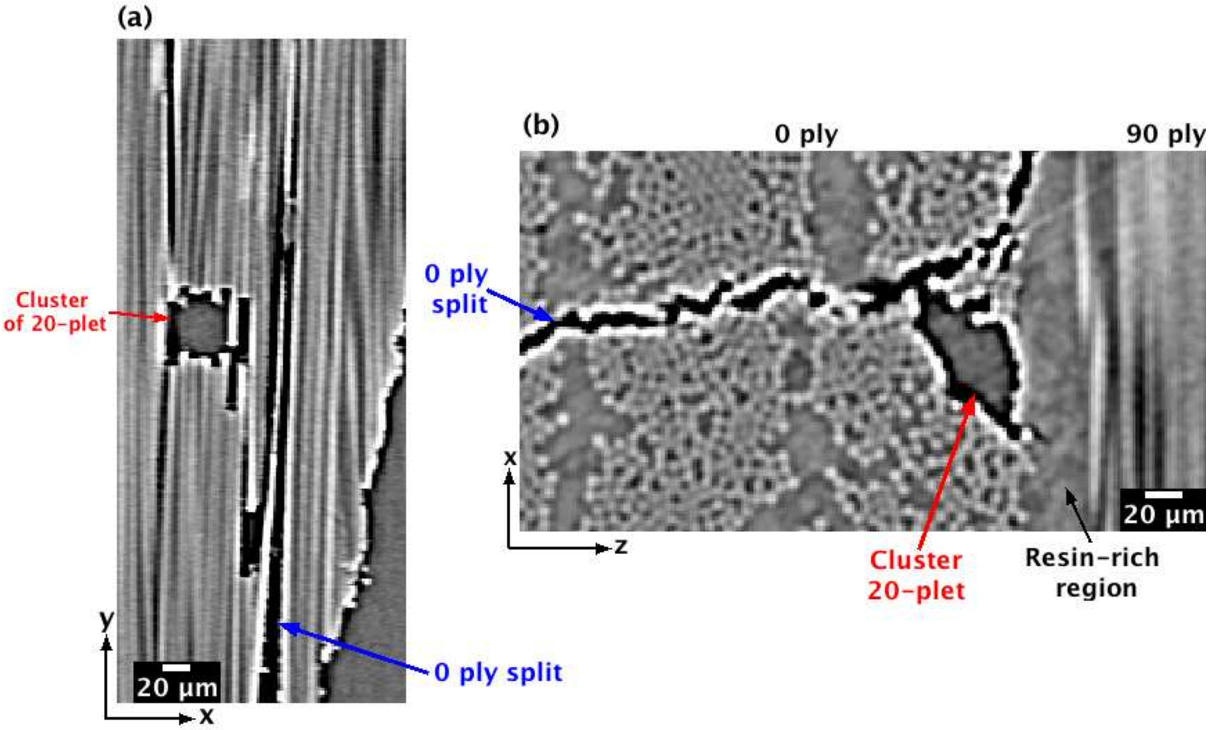
(a)
Cluster
of 20-plet
y
20 µm
x
0 ply split
(b)
0 ply
90 ply
0 ply
split
x
z
20 µm
Cluster
20-plet
Resin-rich
region

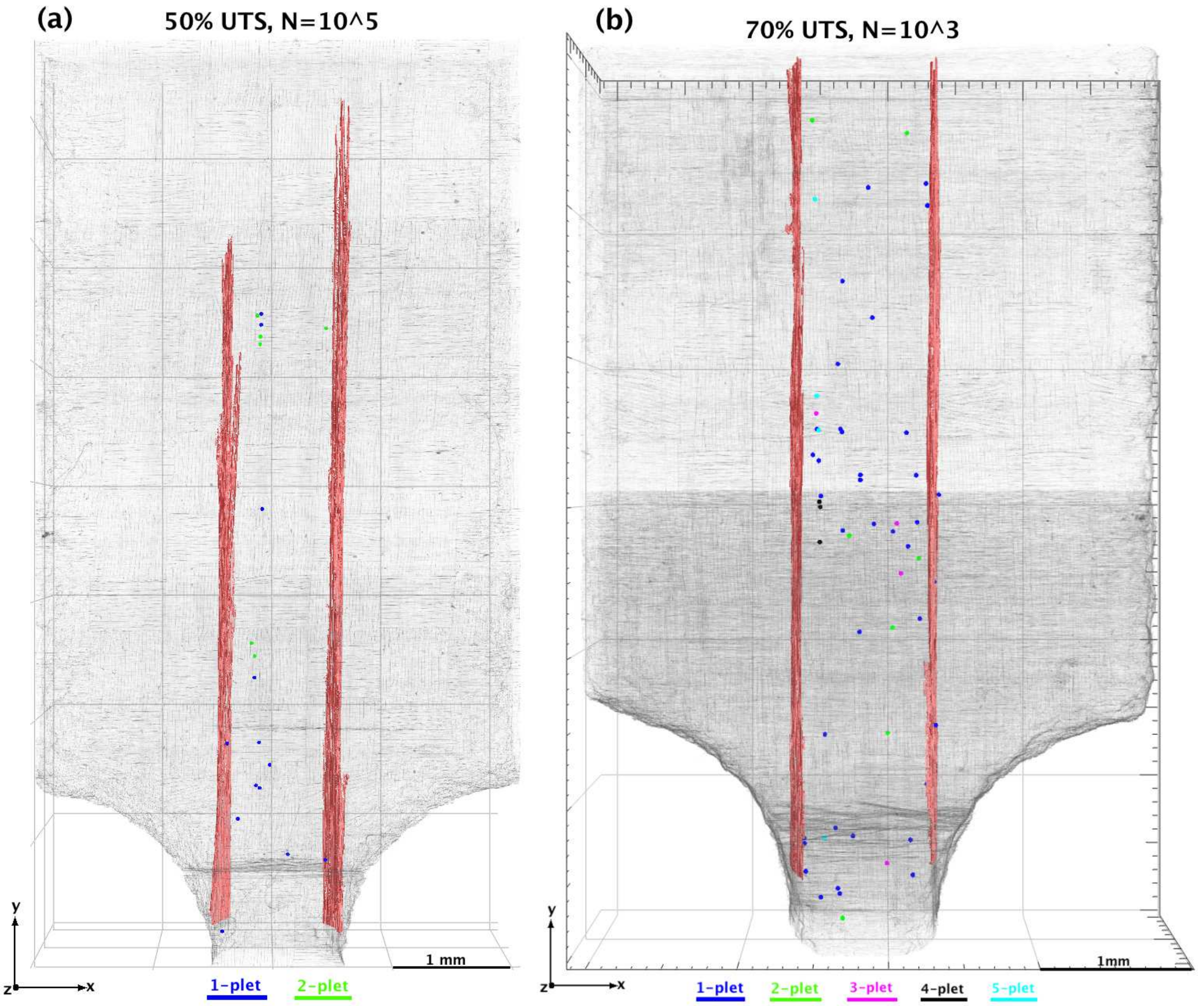

(a)
50% UTS, N=10^5
1 mm
y
z
x
1-plet
2-plet
(b)
70% UTS, N=10^3
1mm
y
z
x
1-plet
2-plet
3-plet
4-plet
5-plet

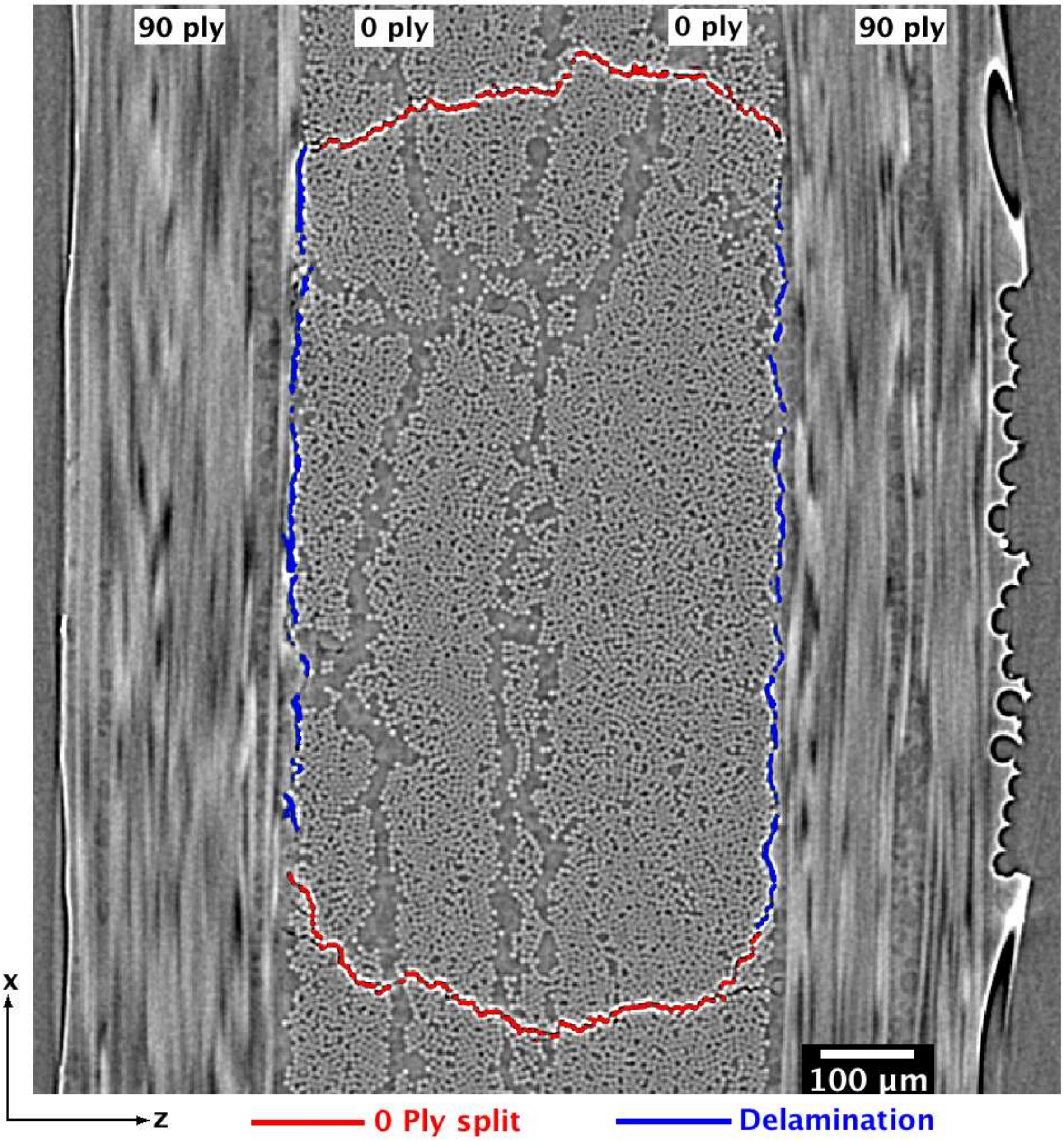

90 ply
0 ply
0 ply
90 ply
100 µm
x
z
0 Ply split
Delamination

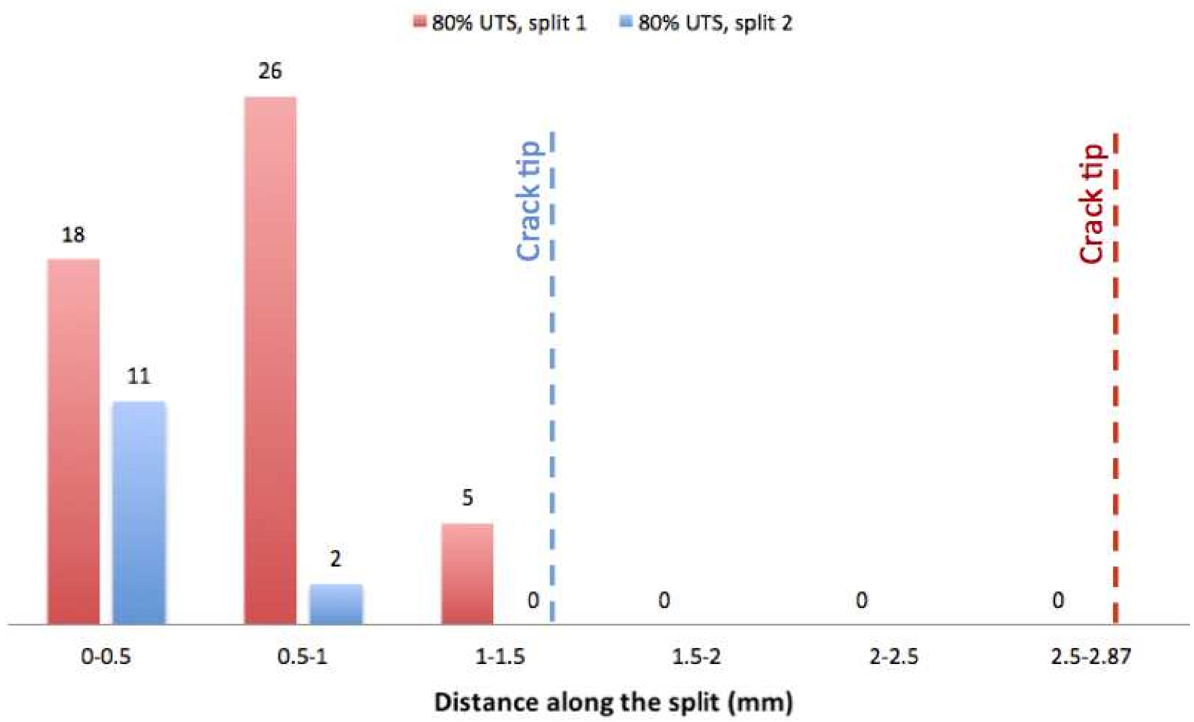

80% UTS, split 1
80% UTS, split 2
26
18
11
5
2
0
0
0
0
Crack tip
Crack tip
0-0.5
0.5-1
1-1.5
1.5-2
2-2.5
2.5-2.87
Distance along the split (mm)